

Universal quantum computation based on Nano-Electro-Mechanical Systems

Motohiko Ezawa,¹ Shun Yasunaga,² Akio Higo,² Tetuya Iizuka,² and Yoshio Mita²

¹*Department of Applied Physics, The University of Tokyo, 7-3-1 Hongo, Tokyo 113-8656, Japan*

²*Department of Electrical Engineering, University of Tokyo, Hongo 7-3-1, 113-8656, Japan*

We propose to use a buckled plate as a qubit, where a double-well potential is mechanically produced by pushing the plate from both the sides. The right and left positions of the plate are assigned to be quantum states $|0\rangle$ and $|1\rangle$. Quantum effects emerge when the displacement is of the order of picometers, although the size of a buckled plate is of the order of $1\mu\text{m}$. The NOT gate is executed by changing the buckling force acting on the plate, while the Pauli-Z gate and the phase-shift gate are executed by applying electric field. A two-qubit phase shift gate is materialized with the use of an electrostatic potential. They constitute a set of universal quantum gates. An examination of material parameters leads to a feasibility of a NEMS(Nano-Electro-Mechanical System)-based quantum computer.

Introduction. According to Moor's law, elements of integrated circuits become exponentially small as a function of year. The size will become the order of nanometers within 10 years, where quantum mechanical effects are inevitable. For example, the superposition of states and the entanglement occur, which are absent in classical mechanics. It is impossible to decrease the size of elements smaller than 1nm , which is a typical scale of atoms. This is the end of Moore's law. Quantum computation[1–3] is a candidate of "More than Moore", which resolves the limit of Moor's law. It gives an exponential speed up for some algorithms. The problem is how to materialize a qubit based on actual materials. Various proposals are made such as superconductors [4], photonic systems [5], quantum dots [6], trapped ions [7], and nuclear magnetic resonance [8, 9]. Recently, nanoscale-skyrmion-based qubits[10, 11] and meron-based qubits[12] are also proposed.

Micro-Electro-Mechanical System (MEMS) is one of the basic elements in the current technology[13–15]. They use electrostatic energy to induce mechanical motions. If the size becomes of the order of nanometer, they are called Nano-Electro-Mechanical System (NEMS)[16, 17]. It has been demonstrated[18–20] that quantum effects emerge in the oscillation modes of a cantilever when its sample size is of the order of $100\text{nm}\sim 1\mu\text{m}$ but with the displacement being of the order of picometers. It is described by a quantum harmonic oscillator. Carbon nanotubes, DNAs or biomolecules are used to compose elements in NEMS. Quantum effects have also been observed for a buckled beam made of a carbon nanotube as in the case of a cantilever .

The buckled plate has two stable positions. It can be used as a classical bit. It has been proposed that an Ising annealing machine is executable by a series of the buckled plates[21]. Its mechanism is based on the electrostatic potential inducing the Ising interaction between two adjacent plates.

A buckled plate would also reveal quantum effects when the displacement is of the order of picometers. In this paper, we propose to use it as a quantum bit, which is well described by a double-well potential. We then propose how to construct a set of universal quantum gates based on buckled plate MEMS, which consists of the phase-shift gate, the Hadamard gate and the CNOT gate. They are constructed by tuning the tension, applying electric field and voltage. A merit is that it is not necessary to use external magnetic field.

Buckled plate MEMS. In the field of MEMS, the bistable structure has been studied with a typical application to memories[1, 21, 23], where a plate is buckled. It was proposed[21] to use this buckled plate as the classical bit information 1 (0), when it is buckled rightward (leftward).

We push a plate from both the ends. The position along the x axis is determined as $x = a$ by minimizing the double-well potential[21, 24] $V_{\text{DW}}(x)$,

$$V_{\text{DW}}(x) = \lambda(x^2 - a^2)^2. \quad (1)$$

Explicit representations of λ and a are given in terms of material parameters in Supplemental Material I.

This buckled plate is an example of a MEMS (NEMS), when its size is of the order of micrometers (nanometers).

Quantum NEMS. The dynamics of a buckled NEMS is described by the Schrödinger equation

$$i\hbar \frac{d}{dt} \psi(x, t) = H \psi(x, t), \quad (2)$$

where the Hamiltonian is

$$H = -\frac{\hbar^2}{2m} \frac{d^2}{dx^2} + V_{\text{DW}}(x), \quad (3)$$

together with the double-well potential (1). In what follows, we use $t_u = (m^2/\hbar\lambda)^{1/3}$ and $x_u = \hbar^{1/3}/(m\lambda)^{1/6}$ as the units of time and space, respectively, about which we explain in Fig.S2 in Supplemental Material II.

Qubit. We numerically solve the eigenenergies of the double-well system[25, 26], and obtain the energy spectrum as in Fig.1(a1). As is well known, it consists of undegenerated levels for small a ($a/x_u \ll 1$) and two-fold degenerated levels for large a ($a/x_u \gg 1$). What is unexpected is a sharp transition of the spectrum at $a \approx 1.5x_u$ as a function of a . We propose to use the lowest two-fold degenerated states at $a \gtrsim 1.5x_u$ as a qubit. Corresponding wavefunctions are shown in Supplemental Material III.

We represent the state $|0\rangle$ by the wave function $\psi_+(x)$ localized at the right bottom and the state $|1\rangle$ by the wave function $\psi_-(x)$ localized at the left bottom. Their degeneracy is resolved for $a \lesssim 1.5x_u$, where the ground state is well described by the symmetric state $(\psi_+ + \psi_-)/\sqrt{2}$. We propose to use this transition of the level splitting at $a \approx 1.5x_u$ for a NOT gate operation.

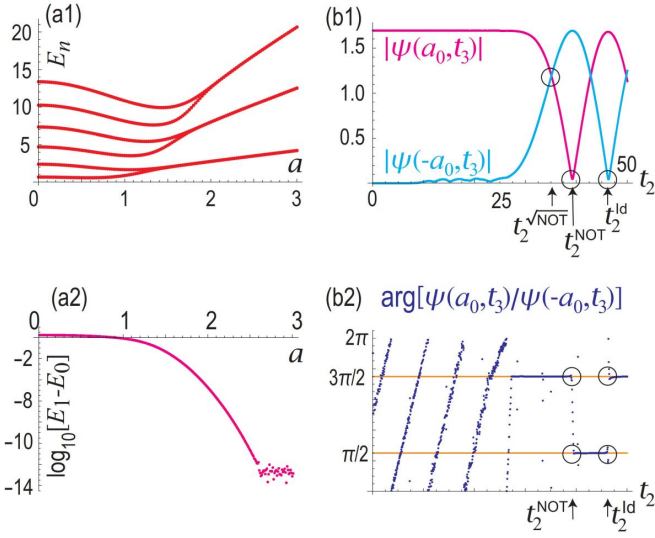


FIG. 1. (a1) The energy spectrum as a function of a . The lowest six energy levels are shown. (a2) The logarithm plot $\log_{10}(E_1 - E_0)$ of the energy difference between the ground state and the first excited state. (b1) The absolute value $|\psi(\pm a_0, t_3)|$ and (b2) The phase difference $\arg\psi(a_0, t_3) - \arg\psi(-a_0, t_3)$. The horizontal axis is the position a in units of x_u in (a1) and (a2), and the time t in units of t_u in (b1) and (b2). We have set $\mathcal{T} = t_u/5$.

Actually, the two-fold degeneracy is slightly broken for finite a . The energy difference between the ground state and the first-excited state is calculated. The $\log_{10}(E_1 - E_0)$ is plotted in Fig.1(a2). It is found that the energy difference is as tiny as $10^{-14}\hbar\sqrt{\lambda/m}$ at $a \approx 2.5x_u$.

The potential is expanded by the harmonic potential

$$V_{\text{DW}}(x) \simeq 4a^2\lambda(x \mp a)^2 + o((x \mp a)^3) \quad (4)$$

in the vicinity of $x = \pm a$ with $a \gtrsim 2x_u$, where the ground-state wave function is given by

$$\psi_{\pm}(x) = \left(\frac{m\omega}{\hbar\pi}\right)^{1/4} \exp\left(-\frac{m\omega}{2\hbar}(x \mp a)^2\right), \quad (5)$$

with the characteristic frequency $\omega = 2a\sqrt{2\lambda/m}$ and the ground state energy $E_0 = \hbar\omega/2$.

Universal quantum gates. It is known that a set of the $\pi/4$ phase-shift gate, the Hadamard gate and the CNOT gate is enough for constructing any quantum circuits. It is known as the Solovay-Kitaev theorem of universal quantum computation[27–29]. We explicitly show that they are actually constructed in buckled NEMS.

Construction of $\sqrt{\text{NOT}}$ and NOT gates. Our scenario reads as follows. Let us start with either the state $|0\rangle$ or $|1\rangle$ at $a = a_0 \gtrsim 2x_u$. For definiteness we take $a_0 = 3x_u$. When we change adiabatically the stable position a from a_0 to $a = 0$, the state is moved to the symmetric state. Then, we change adiabatically the position a back to the point a_0 . More explicitly, by pushing the plate from the both ends, we temporally control the stable position a according to a smooth function,

$$a(t) = \frac{a_0}{2} \left[\tanh\frac{t-t_2}{\mathcal{T}} - \tanh\frac{t-t_1}{\mathcal{T}} + 2 \right], \quad (6)$$

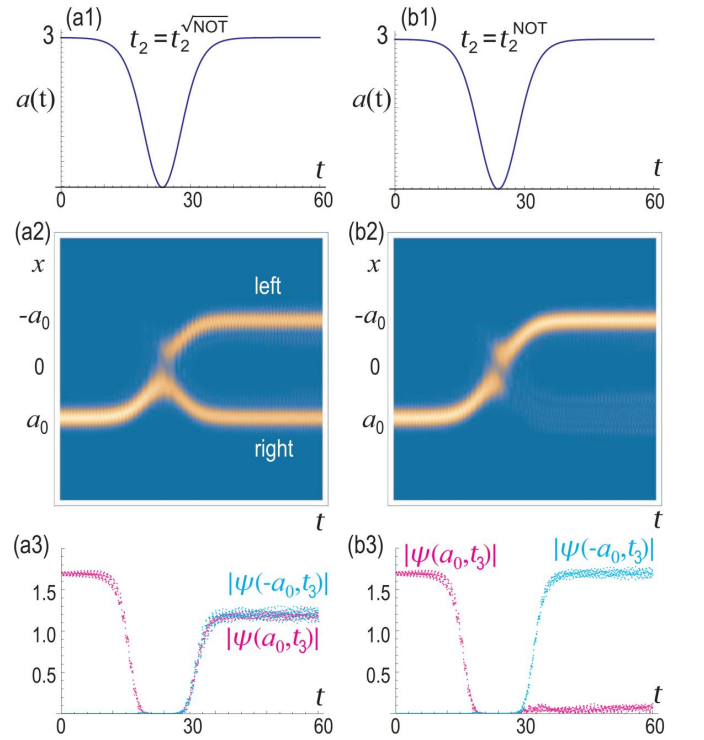


FIG. 2. (a) The $\sqrt{\text{NOT}}$ gate, where we have set $t_2^{\sqrt{\text{NOT}}} = 27.02t_u$. (b) The NOT gate, where we have set $t_2^{\text{NOT}} = 28.87t_u$. (a1) and (b1) The time evolution of $a(t)$ given in Eq.(6) in units of x_u . (a2) and (b2) The time evolution of the spatial profile of the absolute value of the wave function $\psi(x, t)$ starting from the localized state at the right hand side. (a3) and (b3) The time evolution of $|\psi(\pm a_0, t)|$, where $|\psi(a_0, t)|$ colored in magenta and $|\psi(-a_0, t)|$ is colored in cyan. We have set $a_0 = 3x_u$, $t_1 = 20t_u$ and $\mathcal{T} = t_u/5$. The horizontal axis is time ranging $0 < t < 60t_u$.

with three parameters t_1 , t_2 and \mathcal{T} . The resultant state needs not be the state $|0\rangle$ or $|1\rangle$ but can be a combination of $|0\rangle$ and $|1\rangle$ in general.

We study the dynamics of the wave packet by numerically solving the Schrödinger equation (2) with a time-dependent Hamiltonian (3), where the double-well potential (1) is time-dependent with the use of the time-dependent position (6).

We start from the initial state ψ_+ given by Eq.(5) localized at the right-hand side. In order to see the result of the gate operation, we focus on the state $\psi(x, t)$ after enough time of the gate operation at $t = t_3 \gg t_2$. We show the amplitudes $|\psi(\pm a_0, t_3)|$ and the phase shifts $\arg\psi(\pm a_0, t_3)$ as a function of t_2 in Fig.1(b1) and (b2), respectively. We have found that the amplitude changes as a function of t_2 significantly. We also find that the phase difference is $\pi/2$ and $3\pi/2$ shown in Fig.1(a2). The jumps occur where the $|\psi(\pm a_0, t_3)| = 0$.

$\sqrt{\text{NOT}}$ gate: We first construct the square-root NOT gate,

$$U_{\sqrt{\text{NOT}}}^{\pm} = \frac{1}{\sqrt{2}} \left(e^{i\pi/4} I_2 \pm e^{-i\pi/4} \sigma_x \right), \quad (7)$$

which satisfies $\left(U_{\sqrt{\text{NOT}}}^{\pm} \right)^2 = \pm \sigma_x$. We observe in Fig.1(b1) that the amplitude $|\psi(a_0, t)|$ at the initial position colored in

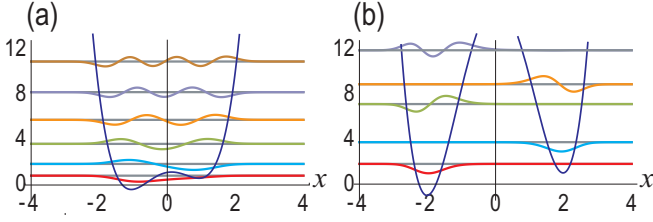


FIG. 3. The wave functions and the energy spectrum under electric field. (a) $a = x_u$ and (b) $a = 2x_u$. The ground state wave function is colored in red, while the first-excited states wave function is colored in cyan. We have set $E_x = 0.5$ in units of $E_u \equiv \hbar\omega/a_0$.

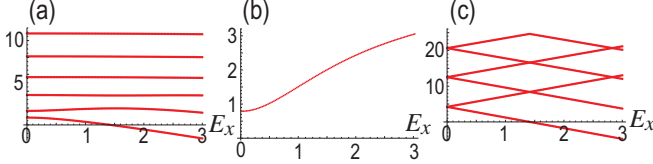


FIG. 4. The energy spectrum as a function of the applied electric field E_x in the case of (a) $a = x_u$ and (c) $a = 3x_u$ (b) The energy difference between the ground state and the first excited state in the case of $a = x_u$. The horizontal axis is E_x in units of $E_u \equiv \hbar\omega/a_0$

magenta decreases for $t_2 > 26t_u$, and it becomes identical to $|\psi(-a_0)|$ colored in cyan at $t_2^{\sqrt{\text{NOT}}} = 27.02t_u$. This value of the parameter is special, where we study the time evolution of the spatial profile. The result is given in Fig.2(a2), where the wave packet is split equally to the right and left positions. The time evolution of the amplitude at $x = \pm a_0$ is shown in Fig.2(a3). We find that the wave function becomes stationary after the gate operation for $t \gtrsim 40t_u$. Precisely in the same way, the equal splitting occurs when we start from the initial state ψ_- given by Eq.(5) localized at the left-hand side. This gate operation at $t_2^{\sqrt{\text{NOT}}}$ is summarized as $U_{\sqrt{\text{NOT}}}^{\pm}$.

NOT gate: Next, we construct the NOT gate $U_{\text{NOT}} \equiv \sigma_x$. We observe in Fig.1(b1) that the amplitude $|\psi(a_0, t)|$ at the initial position colored in magenta becomes zero at $t_2^{\text{NOT}} = 28.87t_u$. This value of the parameter is also special, where the wave packet moves to the left position as shown in Fig.2(b2). The corresponding time evolution of the amplitude at $x = \pm a_0$ is shown in Fig.2(b3). This is the NOT gate σ_x . We find that the wave function becomes stationary after the gate operation for $t \gtrsim 40t_u$.

Construction of phase-shift and Pauli-Z gates. We proceed to construct the phase-shift gate. We apply an electric field along the x direction to the buckled plate, where the potential is given by $E_x x$. The potential and eigenfunctions under electric field, $V_{\text{DW}}(x) + E_x x$, are shown in Fig.3. We numerically evaluate the energy spectrum as a function of the electric field, which is shown in Fig.4(a). The energy difference between the ground state and the first-excited state monotonically increases as the increase of electric field as shown in Fig.4(b). For $a_0 = 3x_u$, the energy spectrum changes linearly as a function of the electric field as shown in Fig.4(c). In the first-order perturbation theory, the energy is

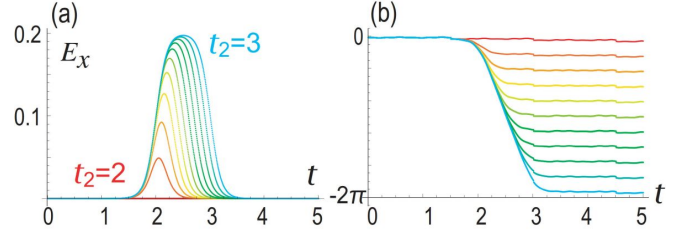


FIG. 5. (a) The time dependence of the applied electric field according to (9) E_x . (b) The time evolution of the phase difference compared with the phase evolution without electric field. The color indicates the time t_2 ranging from $t_2 = 2t_u$ colored in red to $t_2 = 3t_u$ colored in cyan. We have set $t_1 = 2t_u$. The horizontal axis is time ranging $0 < t < 5t_u$. We have set $\mathcal{T} = t_u/5$.

estimated as

$$\langle \psi_{\pm} | E_x x | \psi_{\pm} \rangle = \pm E_x a_0, \quad (8)$$

which is consistent with the numerical results shown in Fig.4(c). Namely, the energy-shift (8) is represented by the effective Hamiltonian $H_{E_x} = a_0 E_x \sigma_z$.

We have numerically evaluated the dynamics of the wave packet starting from the Gaussian distribution (5) under the temporally controlled electric field according to the formula

$$E_x(t) = \frac{E_0}{2} \left[\tanh \frac{t-t_1}{\mathcal{T}} - \tanh \frac{t-t_2}{\mathcal{T}} \right], \quad (9)$$

as shown in Fig.5(a). We found that the absolute value $|\psi|$ does not change. However, the phase is modulated as in Fig.5(b) for the state $|\psi_+\rangle$. The phase modulation for the state $|\psi_-\rangle$ is precisely opposite of that of the state $|\psi_+\rangle$. Hence, the result is summarized as the unitary operator

$$U_Z(\theta) = \text{diag.} \left(e^{-i\theta/2}, e^{i\theta/2} \right) = \exp \left[-\frac{i\theta}{2} \sigma_z \right], \quad (10)$$

where θ is determined as a function of t_2 as illustrated in Fig.5(b). This is the phase-shift gate by angle θ .

$\pi/4$ phase-shift gate: The $\pi/4$ phase-shift gate $U_T \equiv \text{diag.}(1, e^{i\pi/4})$ is realized by the z rotation (10) with the angle $\theta = \pi/4$ as $U_T = e^{-i\pi/8} U_Z(\pi/4)$ up to the overall phase factor $e^{i\pi/8}$.

Pauli-Z gate: The Pauli-Z gate is realized by the z rotation with the angle π as $U_Z = -iU_Z(\pi)$ in a similar way.

The Hadamard gate. The Hadamard gate is defined by $U_H \equiv (\sigma_z + \sigma_x)/\sqrt{2}$. It is realized by a sequential application of the z rotation and the x rotation [30] as

$$U_H = -iU_Z U_{\text{NOT}} U_Z. \quad (11)$$

Two-qubit phase-shift gate. Next, we construct two-qubit gates made of two buckled plates. When we apply the voltage V_1 between the two plates, the potential energy is given by

$$V(x_1, x_2) \equiv V_{\text{DW}}(x_1) + V_{\text{DW}}(x_2) + \frac{C_{\text{para}}(x_1, x_2)}{2} V_1^2, \quad (12)$$

with $C_{\text{para}}(x_1, x_2)$ the capacitance between the plates,

$$C_{\text{para}}(x_1, x_2) = \frac{\varepsilon_0 S}{X_{\text{cap}} + x_1 - x_2}, \quad (13)$$

where ε_0 and S are the permittivity and the plate area, while X_{cap} is the distance between the two plates. We assume that the plate distance X_{cap} is very large compared with the displacement a . We calculate

$$V(a, a) = V(-a, -a) = \frac{\varepsilon_0 S}{X_{\text{cap}}} \frac{V_1^2}{2} \equiv E_0, \quad (14)$$

$$V(a, -a) = \frac{\varepsilon_0 S}{X_{\text{cap}} + 2a} \frac{V_1^2}{2} \equiv E_+, \quad (15)$$

$$V(-a, a) = \frac{\varepsilon_0 S}{X_{\text{cap}} - 2a} \frac{V_1^2}{2} \equiv E_-. \quad (16)$$

Then, the potential differences are given by

$$E_+ - E_0 \simeq -\frac{a}{X_{\text{cap}}^2} \varepsilon_0 S V_1^2 = -E_X, \quad (17)$$

$$E_- - E_0 \simeq \frac{a}{X_{\text{cap}}^2} \varepsilon_0 S V_1^2 = E_X. \quad (18)$$

The detailed derivation is shown in Supplemental Material IV.

We start with the Gaussian state $\Psi_{\sigma_1 \sigma_2}(x_1, x_2) \equiv \psi_{\sigma_1}(x_1) \psi_{\sigma_2}(x_2)$ with Eq.(5) localized at four points $x_1 = \sigma_1 a$ and $x_2 = \sigma_2 a$, where $\sigma_1 = \pm, \sigma_2 = \pm$. The absolute value of this wave function almost remains as it is for a potential at $a/x_u \gg 1$, but a phase shift occurs. The unitary evolution is given by

$$U(t) = \exp[-i(E_0/\hbar + \omega)t] \quad (19)$$

for $\sigma_1 = \sigma_2 = +$ and $\sigma_1 = \sigma_2 = -$,

$$U(t) = \exp[-i(E_+/\hbar + \omega)t] \quad (20)$$

for $\sigma_1 = +$ and $\sigma_2 = -$,

$$U(t) = \exp[-i(E_-/\hbar + \omega)t] \quad (21)$$

for $\sigma_1 = -$ and $\sigma_2 = +$, where we have added the zero-point energy.

It corresponds to the two-qubit phase-shift gate

$$U_{2\text{-phase}}(t) = \text{diag.} \left(e^{-i\frac{E_0}{\hbar}t}, e^{-i\frac{E_-}{\hbar}t}, e^{-i\frac{E_+}{\hbar}t}, e^{-i\frac{E_0}{\hbar}t} \right) \\ = e^{-i\frac{E_0}{\hbar}t} \text{diag.} \left(1, e^{-i\frac{E_X}{\hbar}t}, e^{i\frac{E_X}{\hbar}t}, 1 \right), \quad (22)$$

by identifying the qubit state $(|00\rangle, |01\rangle, |10\rangle, |11\rangle)^t = (|++\rangle, |+-\rangle, |-+\rangle, |--\rangle)^t$.

Ising gate: The Ising gate $U_{ZZ} \equiv \text{diag.}(1, -1, -1, 1)$, by setting $E_X t/\hbar = \pi$ up to the global phase $\exp[-iE_0 t/\hbar]$.

CZ gate: The controlled-Z (CZ) gate U_{CZ} is a unitary operation acting on two adjacent qubits defined by $U_{CZ} = \text{diag.}(1, 1, 1, -1)$. We construct it by a sequential application of the Ising gate and the one-qubit phase-shift gates as[31]

$$U_{CZ} = e^{i\pi/4} U_Z \left(\frac{\pi}{2} \right) U_Z \left(\frac{\pi}{2} \right) U_{ZZ}, \quad (23)$$

By using the results (S19) and (18), it is enough to set $\phi_1 = \pi - \phi_2 = E_X t/\hbar$ to construct the CZ gate.

CNOT gate: The CNOT is constructed by a sequential application of the CZ gate (23) and the Hadamard gate (11) as $U_{\text{CNOT}}^{1 \rightarrow 2} = U_{\text{H}}^{(2)} U_{\text{CZ}} U_{\text{H}}^{(2)}$. See the definition of the CNOT gate in Supplemental Material V.

Discussions. We would like to address the feasibility of a NEMS-based quantum computer by examining typical material parameters[19]. The length of an element is of the order of $1\mu\text{m} \sim 100\mu\text{m}$. The displacement is of the order of $0.1\text{pm} \sim 10\text{fm}$. The mass m is of the order of $10^{-21}\text{kg} \sim 10^{-14}\text{kg}$. The characteristic frequency is of the order of $\sqrt{\kappa/m}$, or $1\text{MHz} \sim 1\text{GHz}$. Then, such a NEMS-based quantum computer would be realizable by improving the present technology.

M.E. is grateful to N. Nagaosa for helpful discussions on the subject. This work is supported by CREST, JST (Grants No. JPMJCR20T2).

[1] R. Feynman, Simulating physics with computers, Int. J. Theor. Phys. **21**, 467 (1982).
 [2] D. P. DiVincenzo, Quantum Computation, Science **270**, 255 (1995).
 [3] M. Nielsen and I. Chuang, "Quantum Computation and Quantum Information", Cambridge University Press, (2016); ISBN 978-1-107-00217-3.
 [4] Y. Nakamura; Yu. A. Pashkin; J. S. Tsai, Coherent control of macroscopic quantum states in a single-Cooper-pair box, Nature **398**, 786 (1999).
 [5] E. Knill, R. Laflamme and G. J. Milburn, A scheme for efficient quantum computation with linear optics, Nature, **409**, 46 (2001).
 [6] D. Loss and D. P. DiVincenzo, Quantum computation with quantum dots, Phys. Rev. A **57**, 120 (1998).
 [7] J. I. Cirac and P. Zoller, Quantum Computations with Cold

Trapped Ions, Phys. Rev. Lett. **74**, 4091 (1995).
 [8] L. M.K. Vandersypen, M. Steffen, G. Breyta, C. S. Yannoni, M. H. Sherwood, I. L. Chuang, Experimental realization of Shor's quantum factoring algorithm using nuclear magnetic resonance, Nature **414**, 883 (2001).
 [9] B. E. Kane, A silicon-based nuclear spin quantum computer, Nature **393**, 133 (1998).
 [10] C. Psaroudaki and C. Panagopoulos, Skyrmion Qubits: A New Class of Quantum Logic Elements Based on Nanoscale Magnetization, Phys. Rev. Lett. **127**, 06720 (2021).
 [11] J. Xia, X. Zhang, X. Liu, Y. Zhou, M. Ezawa, Universal quantum computation based on nanoscale skyrmion helicity qubits in frustrated magnets arXiv:2204.04589.
 [12] J. Xia, X. Zhang, X. Liu, Y. Zhou, M. Ezawa, Qubits based on merons in magnetic nanodisks, arXiv:2205.04716.

- [13] Y. Mita, A. Hirakawa, B. Stefanelli, I. Mori, Y. Okamoto, S. Morishita, M. Kubota, E. Lebrasseur, A. Kaiser, *Japanese Journal of Applied Physics* **57**, 04FA05 (2018).
- [14] R. Reddy, K. Komeda, Y. Okamoto, E. Lebrasseur, A. Higo, Y. Mita, *Sensors and Actuators A: Physical*, **295**, 1 (2019).
- [15] H. Toshiyoshi, Electrostatic Actuation. In: Yogesh B Gianchandani, Osamu Tabata, Hans Zappe, (Editors in Chief) *Comprehensive Microsystems*, **2**, 1 Amsterdam: Elsevier. (2008).
- [16] H. G. Craighead, *Science* **290**, 1532 (2000).
- [17] K. L. Ekinci and M. L. Roukes, *Rev. Sci. Instruments* **76**, 6 (2005).
- [18] M. Blencowe, *Physics Reports* **395**, 159 (2004)
- [19] M. Poot, H. S.J. van der Zant, *Physics Reports* **511**, 273 (2012).
- [20] O. Slowik, K. Orłowska, D. Kopiec, P. Janus, P. Grabiec and T. Gotszalk, *Measurement Automation Monitoring, Mar.*, **62**, 2450 (2016).
- [21] M. Ezawa, Eric Lebrasseur and Yoshio Mita, Nonvolatile bistable memory and Ising machine based on Micro-Electro-Mechanical Systems, [app-ph/arXiv:2106.09931](https://arxiv.org/abs/2106.09931).
- [22] M. Vangbo, *Sensors and Actuators A: Physical* **69**, 212 (1998).
- [23] V. Intaraprasong and S. Fan, *Appl. Phys. Lett.* **98**, 241104 (2011).
- [24] J. Martinez-Rincon and Y. V. Pershin, *IEEE Transactions on Electron Devices* **58**, 1809 (2011).
- [25] H. J. Korsch and M. Gluck *Eur. J. Phys.* **23** 413 (2002).
- [26] Solving the eigenvalue problem for a double well potential using a 1D particle in a box as a basis set <https://mathematica.stackexchange.com/questions/187471/solving-the-eigenvalue-problem-for-a-double-well-potential-using-a-1d-particle-i>
- [27] D. Deutsch, Quantum theory, the Church Turing principle and the universal quantum computer, *Proceedings of the Royal Society A*, **400**, 97 (1985).
- [28] C. M. Dawson and M. A. Nielsen, The Solovay-Kitaev algorithm, [quant-ph/arXiv:0505030](https://arxiv.org/abs/0505030).
- [29] M. Nielsen and I. Chuang, "Quantum Computation and Quantum Information", Cambridge University Press, Cambridge, UK (2010).
- [30] N. Schuch and J. Seiwert, Natural two-qubit gate for quantum computation using the XY interaction, *Phys. Rev. A* **67**, 032301 (2003).
- [31] Y. Makhlin, *Quant. Info. Proc.* **1**, 243 (2002).

Supplemental Material

Universal quantum computation based on Nano-Electro-Mechanical Systems

Motohiko Ezawa

Department of Applied Physics, The University of Tokyo, 7-3-1, Hongo, Bunkyo-ku, Tokyo 113-8656, Japan

Shun Yasunaga, Akio Higo, Tetuya Iizuka, Yoshio Mita

Department of Electrical Engineering, University of Tokyo, Hongo 7-3-1, 113-8656, Japan

I. BUCKLED PLATE MEMS

We consider a plate with length $2L_0$ and the spring constant κ placed along the y axis. The form of the buckled plate is determined by the Euler-Bernoulli equation[1, 2],

$$\frac{d^4 w}{dy^4} + m^2 \frac{d^2 w}{dy^2} = 0, \quad (\text{S1})$$

with $m^2 \equiv P/EI$, where P is the axial load, E is Young's modulus of the beam material and I is the second moment of area of the beam. In solving the Euler-Bernoulli equation for a clamped-clamped beam, we may use the fixed boundary condition or the free boundary condition.

First, we impose the fixed boundary condition, which reads

$$w(-y_0) = w(y_0) = 0, \quad \left. \frac{dw}{dy} \right|_{x=-y_0} = \left. \frac{dw}{dy} \right|_{x=y_0} = 0, \quad (\text{S2})$$

where y_0 is the position of the supporting point along the y axis

The lowest energy solution is given by[3]

$$w = \frac{x_0}{2} \left(1 + \cos \frac{\pi y}{y_0} \right), \quad (\text{S3})$$

where x_0 is the position along the x axis. The length of the buckled plate is given by $L(x_0) = \int_{-y_0}^{y_0} dy \sqrt{1 + (dw/dy)^2}$. It is calculated as

$$\begin{aligned} L(x_0) &= \int_{-y_0}^{y_0} dy \sqrt{1 + \frac{\pi^2 x_0^2}{4y_0^2} \sin^2 \frac{\pi y}{y_0}} = \frac{y_0}{\pi} \int_{-\pi}^{\pi} d\theta \sqrt{1 + \frac{\pi^2 x_0^2}{4y_0^2} \sin^2 \theta} \\ &= \frac{4y_0}{\pi} \int_0^{\pi/2} d\theta \sqrt{1 + \frac{\pi^2 x_0^2}{4y_0^2} \sin^2 \theta} = \frac{4y_0}{\pi} E \left(-i \frac{\pi x_0}{2y_0} \right), \end{aligned} \quad (\text{S4})$$

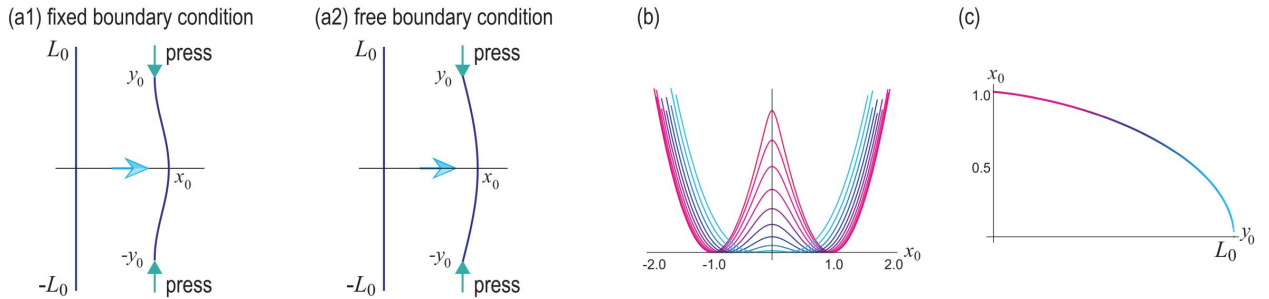


FIG. S1. Illustration of a buckled plate with (a1) fixed boundary condition and (a2) free boundary condition. (b) Electric field is applied along the x direction in order to construct the Pauli-Z gate. (c) The electrostatic potential is induced by applying voltage in order to construct the two-qubit phase-shift gate.

where E is the complete elliptic integral of the second kind defined by

$$E(k) \equiv \int_0^{\pi/2} \sqrt{1 - k^2 \sin^2 \theta} d\theta. \quad (\text{S5})$$

The potential energy is given by the Hooke law

$$V(x_0) = \frac{\kappa}{2} (2L(x_0) - 2L_0)^2, \quad (\text{S6})$$

which we show for various y_0 in Fig.S1(b). It is a double-well potential. The potential minimum is shown as a function of y_0 in Fig.S1(c).

We expand Eq.(S6) in terms of x_0 by fixing L_0 and y_0 as

$$V(x_0) = \frac{\kappa}{2} (2L_0 - 2y_0)^2 + \frac{1}{4y_0} (L_0 - y_0) \kappa \pi^2 x_0^2 + \frac{(L_0 - 3y_0)}{256y_0^3} \kappa \pi^4 x_0^4 + o(x_0^6). \quad (\text{S7})$$

It is summarized as $V(x_0) = \lambda(x_0^2 - a^2)^2 + V_0 + o(x_0^6)$ with

$$\lambda \equiv \frac{(L_0 - 3y_0)}{256y_0^3} \kappa \pi^4, \quad a \equiv y_0 \frac{4\sqrt{2}}{\pi} \sqrt{\frac{L_0 - y_0}{3L_0 - y_0}}. \quad (\text{S8})$$

The parameter x_0 is determined as $x_0 = a$ by minimizing the potential $V(x_0)$. This buckled plate is an example of a MEMS (NEMS), when its size is of the order of micrometers (nanometers).

Second, we impose the fixed boundary condition, which reads

$$\left. \frac{d^2 w}{dy^2} \right|_{x=-y_0} = \left. \frac{d^2 w}{dy^2} \right|_{x=y_0} = 0, \quad (\text{S9})$$

whose solution is[4]

$$w = x_0 \cos \frac{\pi y}{2y_0}. \quad (\text{S10})$$

The length $L(x_0)$ is given by Eq.(S4) precisely as in the case of the fixed boundary condition. Hence, the potential energy is given by the same Hooke law as Eq.(S6).

II. UNITS OF TIME AND SPACE

It is straightforward to rewrite the Schrödinger equation (2) and the Hamiltonian (3) in the main text as

$$i \frac{d}{d\tau} \psi(X, \tau) = H \psi(X, \tau) \quad (\text{S11})$$

and

$$H = -\frac{1}{2} (d/dX)^2 + (X^2 - A^2)^2 \quad (\text{S12})$$

in terms of the dimensionless time $\tau = t/t_u$ and the dimensionless parameters $X \equiv x/x_u$ and $A \equiv a/x_u$, where $t_u = (m^2/\hbar\lambda)^{1/3}$ and $x_u = \hbar^{1/3}/(m\lambda)^{1/6}$ give the units of time and space, respectively. We have carried out numerical analysis based on the dimensionless formulas.

III. WAVEFUNCTION

We also numerically determine the wave functions for a double-well potential, which are shown in Fig.S2. They are well described by those of the harmonic potential for large a .

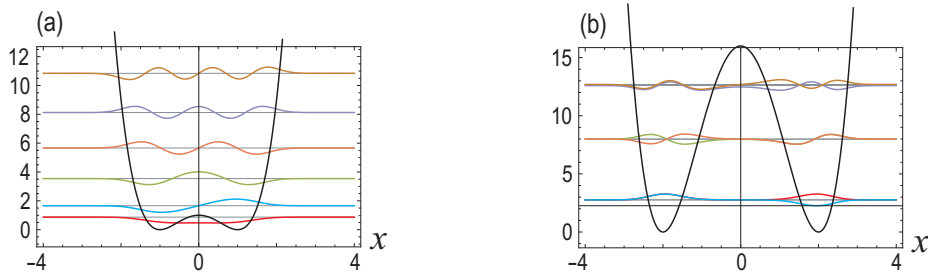


FIG. S2. Wave functions and energy spectrum with varying stress. (a) $a = x_u$, (b) $a = 2x_u$ and (c) $a = 3x_u$. The horizontal axis is x . The ground state wave function is colored in red, while the first-excited states wave function is colored in cyan.

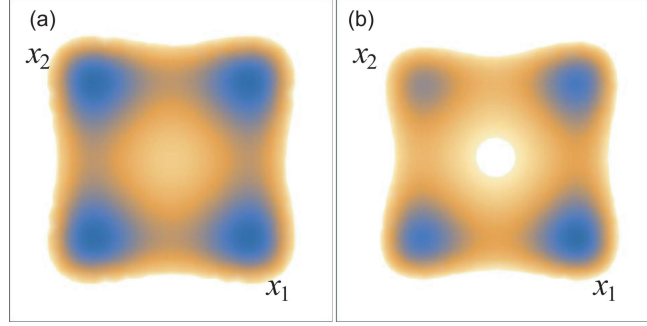


FIG. S3. Density plot of energy spectrum (S15) in the x_1 - x_2 plane. (a) Zero voltage $V_1 = 0$. (b) Nonzero voltage $\varepsilon_0 S V_1^2 / 2 = 100$. We have set $X_{\text{cap}} = 10x_u$ and $a = 2x_u$.

IV. ELECTROSTATIC ENERGY

In the parallel-plate NEMS, the capacitance between the plates x_1 and x_2 is well described by

$$C_{\text{para}}(x_1, x_2) = \frac{\varepsilon_0 S}{X_{\text{cap}} + x_1 - x_2}, \quad (\text{S13})$$

where X_{cap} is the distance between the adjacent plates without buckling, S is the area of the plate, and ε_0 is the permittivity. The electrostatic potential is given by

$$U_{\text{cap}} = \frac{C_{\text{para}}(x_1, x_2)}{2} V_1^2, \quad (\text{S14})$$

when we control the voltage V_1 between the plates.

We consider a set of two adjacent plates, where the potential energy is given by

$$V(x_1, x_2) \equiv V(x_1) + V(x_2) + \frac{C_{\text{para}}(x_1, x_2)}{2} V_1^2. \quad (\text{S15})$$

We show the potential in the x_1 - x_2 plane in Fig.S3. In the absence of the applied voltage $V_1 = 0$, there are four-fold degenerated bottoms at $u_1 = \pm a$ and $u_2 = \pm a$ as shown in Fig.S3(a), where the ground state energy is $\hbar\omega$. Under applied voltage, they are split as

$$V(a, a) = V(-a, -a) = \frac{\varepsilon_0 S}{X_{\text{cap}}} \frac{V_1^2}{2} \equiv E_0, \quad (\text{S16})$$

$$V(a, -a) = \frac{\varepsilon_0 S}{X_{\text{cap}} + 2a} \frac{V_1^2}{2} \equiv E_+, \quad (\text{S17})$$

$$V(-a, a) = \frac{\varepsilon_0 S}{X_{\text{cap}} - 2a} \frac{V_1^2}{2} \equiv E_-. \quad (\text{S18})$$

We also plot the potential profile with nonzero voltage in Fig.S3(b). We assume that the plate distance X_{cap} is very large compared with the deviation a and obtain

$$E_+ - E_0 \simeq -\frac{a}{X_{\text{cap}}^2} \varepsilon_0 S V_1^2, \quad E_- - E_0 \simeq \frac{a}{X_{\text{cap}}^2} \varepsilon_0 S V_1^2. \quad (\text{S19})$$

V. CNOT GATES

The CNOT gate $U_{\text{CNOT}}^{1 \rightarrow 2}$ is defined by

$$U_{\text{CNOT}}^{1 \rightarrow 2} \equiv \begin{pmatrix} 1 & 0 & 0 & 0 \\ 0 & 1 & 0 & 0 \\ 0 & 0 & 0 & 1 \\ 0 & 0 & 1 & 0 \end{pmatrix}, \quad (\text{S20})$$

where the first qubit is the controlled qubit and the second qubit is the target qubit.

-
- [1] M. Vangbo and Y. Baklund, *J. Micromechanics and Microengineering*, **8**, 29 (1998)
 - [2] M. Vangbo, *Sensors Actuators A* **69**, 212 (1998)
 - [3] B. Charlot, W. Sun, K. Yamashita, H. Fujita and H. Toshiyoshi, *J. Micromech. Microeng.* **18**, 045005 (2008)
 - [4] T. N. Binh, S. Morishita, M. Kubota and Y. Mita, 2012 International Conference on Optical MEMS and Nanophotonics